Received: 30 June 2023 | Revised: 8 December 2023 | Accepted: 18 December 2023

DOI: 10.1002/pamm.202300146

RESEARCH ARTICLE

Preserving mesh quality in shape optimization

Sofiya Onyshkevych | **Martin Siebenborn** | **Winnifried Wollner**

Department of Mathematics, University of Hamburg, Hamburg, Germany

Correspondence
Sofiya Onyshkevych, Department of Mathematics, University of Hamburg, Bundesstraße 55, 20146 Hamburg, Germany.
Email: sofiya.onyshkevych@uni-hamburg.de

Abstract

In PDE-constrained shape optimization, a lot of computational effort is used to update the geometry at every iteration step. This iterative process can result in loss of element quality and degeneracy of the underlying mesh, which is particularly relevant for applications involving large deformations of some parts of the domain. To avoid remeshing, we model the mesh deformation using the method of mappings. We use an extension equation that maps a boundary control variable to a deformation field defined over the entire domain. By using the nonlinear extension operator proposed in our previous work, we increase the set of reachable shapes, allowing us to model large deformations. We discuss how the choice of parameters of the extension equations affects the mesh quality and we study the influence of the extension factor on the convergence properties of the iterative solvers.

1 | INTRODUCTION

In industrial applications, the problem of optimizing the shape of an object with respect to a certain objective function often arises. Mathematically, these problems are formulated as shape optimization problems: one strives to optimize a shape of the design, subject to some physical constraints, typically described by partial differential equations (PDEs).

Shape optimization problems with PDE constraints have been studied in acoustics [2, 3], magnetostatics [4], composite material identification [5, 6], nano-optics [7], and other areas.

We are considering shape optimization problems of the type

$$\begin{aligned} \min_{\Omega \in G_{\text{adm}}} \quad & j(y, \Omega) \\ \text{s.t.} \quad & E(y, \Omega) = 0 \end{aligned} \tag{1}$$

where j is a shape functional depending on a state variable y and the shape of the domain Ω, and $E(y, \Omega) = 0$ is a PDE with solution y defined over the domain $\Omega \subset \mathbb{R}^d, d = 2, 3$.

There are several different approaches to tackle such problems. One can consider the problem strictly from the shape calculus perspective and study the Eulerian derivative of shape functionals $J(\Omega)$ applying the Hadamard–Zolésio theorem and using the Hadamard representation of the shape gradient [8, 9].

The viewpoint we are going to follow here is to consider the problem as an optimal control problem with the control being the deformation of the design boundary. We then derive the optimality system by differentiating the Lagrangian

of the problem and solve by applying gradient-based optimization methods. So instead of applying shape calculus, we compute the shape gradient via the adjoint equation, which is already a part of our optimality system.

In shape optimization methods, the geometry changes at every optimization step. Hence the algorithm should recompute the mesh at every iteration, which can be done via remeshing or mesh deformation. Remeshing methods are known to produce good quality meshes, which are stable under any deformation. However, since they are of a high computational cost we are opting to use the mesh deformation methods.

The main idea is to use additional PDEs to compute the deformation of the mesh. One of the most popular choices is the linear elasticity equation [10] with variable Lamé parameters. However under large deformations, the linear elasticity equation often results in degenerated meshes. Hence, we choose a nonlinear equation to compute the mesh deformation following [1].

2 | OPTIMIZATION PROBLEM

In this article, as an underlying physical model, we consider the classical problem of fluid dynamics.

We consider a flow goverened by the incompressible Navier–Stokes equations in a tunnel and an obstacle immersed in this flow. For simplicity, we are going to consider the stationary case only.

The objective is to minimize the energy dissipation functional

$$\min_{\Gamma_{\text{obs}}} \; j(v, \Gamma_{\text{obs}}) = \frac{\nu}{2} \int_{\Omega} \sum_{i,j=1}^{d} \left(\frac{\partial v_i}{\partial x_j} \right)^2 dx, \tag{2}$$

where the contour Γ_{obs} of the obstacle Ω_{obs} is assumed to be variable. We additionally assume that Ω_{obs} is a nonempty, connected set, and Γ_{obs} is a smooth and compact Riemannian manifold without a boundary. Let Ω be a bounded domain in $\mathbb{R}^d$, $d = 2, 3$ with a Lipschitz continuous boundary $\partial\Omega$.

In Equation (2), the flow velocity v is given by stationary Navier–Stokes equations

$$\begin{aligned} -\nu \Delta v + (v \cdot \nabla) v + \nabla p &= 0 && \text{in } \Omega, \\ \operatorname{div} v &= 0 && \text{in } \Omega, \\ v &= v_\infty && \text{on } \Gamma_{\text{in}}, \\ v &= 0 && \text{on } \Gamma_{\text{obs}} \cup \Gamma_{\text{wall}}, \\ pn - \nu \frac{\partial v}{\partial n} &= 0 && \text{on } \Gamma_{\text{out}}, \end{aligned} \tag{3}$$

where $v = v(x) : \Omega \to \mathbb{R}^d$ is the velocity field, $p = p(x) : \Omega \to \mathbb{R}$ is the pressure of the flow at a point x, $n : \Gamma_{\text{out}} \to \mathbb{R}^d$ is the outward-facing unit normal vector to Γ_{out}, ν is a kinematic viscosity, v_∞ is a velocity profile at the inflow boundary.

The setting given by Equation (3) admits the change of the fluid domain and shape of the obstacle, Γ_{obs} and Ω, respectively, but the outer boundaries Γ_{in}, Γ_{out}, and Γ_{wall}, of the experiment are fixed.

Additionally, we assume that Γ_{in} and Γ_{obs} have positive Lebesgue measure, $\Gamma_{\text{obs}} \cap (\Gamma_{\text{in}} \cup \Gamma_{\text{wall}} \cup \Gamma_{\text{out}}) = \emptyset$ holds during the entire optimization.

In order to omit trivial solutions, we additionally introduce geometrical constraints. To prevent the obstacle Ω_{obs} from shrinking and vanishing completely, we fix the volume of the specimen. We also fix the position of the obstacle to avoid the unwanted solution given by the translation of the obstacle towards the walls of the domain. In most numerical examples, for simplicity, we fix the barycenter of the obstacle to be in the middle of the domain.

$$\operatorname{vol}(\Omega_{\text{obs}}) = \int_{\Omega_{\text{obs}}} 1 \, dx = \text{ const}, \tag{4}$$

$$\operatorname{bc}(\Omega_{\text{obs}}) = \frac{1}{\operatorname{vol}(\Omega_{\text{obs}})} \int_{\Omega_{\text{obs}}} x \, dx = \text{ const}. \tag{5}$$

Consider the weak formulation of the PDE constraint given by Equation (3).

Find $(v, p) \in V \times Q$ such that

$$\begin{aligned} \nu \int_\Omega Dv : D\delta_v + (Dv\, v) \cdot \delta_v - p \operatorname{Tr}(D\delta_v)\, dx = 0, \\ - \int_\Omega \delta_p \operatorname{Tr}(Dv)\, dx = 0 \end{aligned} \tag{6}$$

for all test functions $(\delta_v, \delta_p) \in V_0 \times Q$, where

$$\begin{aligned} V &:= \{v \in H^1(\Omega, \mathbb{R}^d) : \operatorname{div}(v) = 0, v|_{\Gamma_{\text{in}}} = v_\infty, v|_{\Gamma_{\text{wall}} \cup \Gamma_{\text{obs}}} = 0 \text{ a.e.}\}, \\ V_0 &:= \{v \in H^1(\Omega, \mathbb{R}^d) : \operatorname{div}(v) = 0, v|_{\Gamma_{\text{in}} \cup \Gamma_{\text{wall}} \cup \Gamma_{\text{obs}}} = 0 \text{ a.e.}\}, \\ Q &:= \{p \in L^2(\Omega)\}. \end{aligned} \tag{7}$$

Now we reformulate the optimization problem on the fixed reference domain by means of the method of mappings. We define the mapping

$$F = \mathrm{id} + w \text{ with } w \in W^{1,\infty}(\Omega, \mathbb{R}^d), \tag{8}$$

where F results in an admissible deformation for Ω. For an in-depth discussion of admissible deformations in shape optimization and the method of mappings, we refer to Refs. [11] and [12], respectively. Here, an admissible deformation belongs to the set of admissible deformations G_{adm}, which in turn leads to shapes in the set of admissible transformations $\mathcal{F}_{\text{adm}}$.

Hence, the weak formulation of the optimization problem on the reference domain Ω is given by

$$\begin{aligned} \min_{F \in \mathcal{F}_{\text{adm}}} \quad & j(v, F(\Omega)) = \frac{\nu}{2} \int_\Omega \left(Dv(DF)^{-1}\right) : \left(Dv(DF)^{-1}\right) \det(DF)\, dx \\ \text{s.t.} \quad & \int_\Omega \Big[\nu \left(Dv(DF)^{-1}\right) : \left(D\delta_v(DF)^{-1}\right) + (Dv(DF)^{-1} v) \cdot \delta_v \\ & \qquad - p \operatorname{Tr}\left(D\delta_v(DF)^{-1}\right)\Big] \det(DF)\, dx = 0, \\ & - \int_\Omega \delta_p \operatorname{Tr}(Dv(DF)^{-1}) \det(DF)\, dx = 0, \\ & \int_{\Omega_{\text{obs}}} \det(DF) - 1\, dx = 0, \\ & \int_{\Omega_{\text{obs}}} F \det(DF)\, dx = 0 \end{aligned}$$

for all test functions $(\delta_v, \delta_p) \in V \times Q$.

3 | NONLINEAR EXTENSION OPERATORS

The only variable we are interested in finding is the deformation field w in Equation (8). We define it via a continuous control-to-deformation mapping S that links a deformation across the whole domain to a control variable defined over the surface of the obstacle Γ_{obs} as follows:

$$w = S(c),$$

where $c \in L^2(\Gamma_{\text{obs}})$ is a design variable. It has been shown in Ref. [12] that for large deformations, that is, when the reference domain and the optimal configuration differ significantly, linear operators S do not lead to satisfying results. Hence, we aim to find a suitable operator S allowing large deformations and not restricting G_{adm}.

In this article, we consider a nonlinear mapping S given in terms of the solution operator of the coupled PDEs following [1]

$$\begin{aligned} b - \Delta_{\Gamma_{\text{obs}}} b &= cn && \text{on } \Gamma_{\text{obs}}, \\ -\operatorname{div}(\nabla w + \nabla w^\top) + \eta_{\text{ext}}(w \cdot \nabla) w &= 0 && \text{in } \Omega, \\ (\nabla w + \nabla w^\top) \cdot n &= b && \text{on } \Gamma_{\text{obs}}, \\ w &= 0 && \text{on } \Gamma_{\text{wall}} \cup \Gamma_{\text{in}} \cup \Gamma_{\text{out}}. \end{aligned} \tag{9}$$

By using the operator S, we link the vector field w defined in the holdall domain and a scalar control variable c defined on the boundary of the obstacle Γ_{obs}.

By having an advection-like nonlinear term in the extension equation (9), we promote the displacements along the tangential directions to the boundary of the obstacle. This way we allow for the tip and a back of the shape to form, allowing for the creation of the necessary geometric singularities.

Further we introduce the weak formulation of Equation (9), where we want to find $(w, b) \in W \times H^2(\Gamma_{\text{obs}})$:

$$\begin{aligned} \int_{\Gamma_{\text{obs}}} b \cdot \delta_b + D_{\Gamma_{\text{obs}}} b \,:\, D_{\Gamma_{\text{obs}}} \delta_b \, ds &= \int_{\Gamma_{\text{obs}}} cn \cdot \delta_b \, ds, \\ \int_\Omega (Dw + Dw^\top) \,:\, D\delta_w + \eta_{\text{ext}}(Dw\, w) \cdot \delta_w \, dx &= \int_{\Gamma_{\text{obs}}} b \delta_w \, ds, \end{aligned} \tag{10}$$

for all $(\delta_w, \delta_b) \in W \times H^2(\Gamma_{\text{obs}})$, where W is defined according to the argumentation in Ref. [12] as follows:

$$W := \left\{ w \in H^{\frac{7}{2}}(\Omega, \mathbb{R}^d) \,:\, w|_{\Gamma_{\text{in}} \cup \Gamma_{\text{wall}} \cup \Gamma_{\text{out}}} = 0 \text{ a.e.} \right\}.$$

Here $D_{\Gamma_{\text{obs}}}$ denotes the derivative tangential to Γ_{obs}, c is the scalar-valued boundary control, and n is the outer normal unit vector to Ω at Γ_{obs}. Additionally, the amount of influence of the nonlinear advection term is determined by η_{ext}. Namely, when $\eta_{\text{ext}} = 0$, the extension equation is linear, which corresponds to the standard linear elasticity approach.

We complete the system with an inequality constraint bounding the determinant of the deformation gradient

$$\det(DF) \geq \eta_{\text{det}} \text{ in } \Omega. \tag{11}$$

It is shown in Ref. [12] that the condition (11) ensures the local injectivity of F by limiting the amount of local change of volume for each element of the mesh. Despite limiting this way a subset of admissible transformations F_{adm}, it was shown in Ref. [1] that the nonlinear extension operator S often prevents this condition from becoming active even for large deformations.

To derive the optimality conditions of the optimization problem, we define the Lagrangian function using the penalty method to enforce geometrical constraints and the determinant condition

$$\begin{aligned} &\mathcal{L}(w, v, p, b, c, \psi_w, \psi_v, \psi_p, \psi_b, \psi_{\text{vol}}, \psi_{\text{bc}}) \\ &= \frac{\nu}{2} \int_\Omega \left(Dv(DF)^{-1}\right) \,:\, \left(Dv(DF)^{-1}\right) \det(DF)\, dx + \frac{\alpha}{2} \int_{\Gamma_{\text{obs}}} c^2 \, ds + \frac{\beta}{2} \int_\Omega ((\eta_{\text{det}} - \det(DF))_+)^2 \, dx \\ &\quad - \int_\Omega \left[\nu \left(Dv(DF)^{-1}\right) \,:\, \left(D\psi_v(DF)^{-1}\right) + (Dv(DF)^{-1} v) \cdot \psi_v - p \operatorname{Tr}\left(D\psi_v(DF)^{-1}\right)\right] \det(DF)\, dx \\ &\quad + \int_\Omega \psi_p \operatorname{Tr}(Dv(DF)^{-1}) \det(DF)\, dx \\ &\quad - \int_\Omega (Dw + Dw^\top) \,:\, D\psi_w + \eta_{\text{ext}}(Dw\, w) \cdot \psi_w \, dx + \int_{\Gamma_{\text{obs}}} b \cdot \psi_w \, ds \\ &\quad - \int_{\Gamma_{\text{obs}}} b \cdot \psi_b + D_{\Gamma_{\text{obs}}} b \,:\, D_{\Gamma_{\text{obs}}} \psi_b \, ds + \int_{\Gamma_{\text{obs}}} cn \cdot \psi_b \, ds \\ &\quad - \psi_{\text{bc}} \cdot \int_\Omega (x + w) \, \det(DF)\, dx - \psi_{\text{vol}} \int_\Omega \det(DF) - 1 \, dx, \end{aligned} \tag{12}$$

where $\psi_\cdot$ is the multiplier associated with each variable.

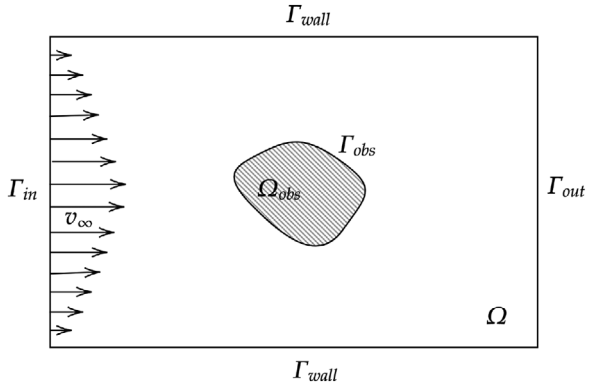

FIGURE 1 Sketch of the holdall domain $G = \Omega \cup \Omega_{\text{obs}}$, tunnel-like domain Ω with the obstacle Ω_{obs} with boundary Γ_{obs}, wall boundaries Γ_{wall}, inflow Γ_{in}, and outflow Γ_{out}.

From Equation (12), we obtain necessary optimality conditions by taking a derivative with respect to every variable.

4 | NUMERICAL RESULTS

In this section, we quantify the quality of the mesh obtained with the nonlinear extension equation and study how it correlates with the condition number and other numerical properties of the problem.

We define the condition number of the Hessian H of the optimization problem as

$$\kappa(H) = \frac{\lambda_{\max}(H)}{\lambda_{\min}(H)}, \tag{13}$$

where $\lambda_{\max}(H), \lambda_{\min}(H)$ are the largest and smallest eigenvalues of H.

It is known that the stability and error of the finite element discretization are affected by the mesh quality, in particular when the angle of an element becomes too small the condition number of finite element matrix increases [13, 14]. Further the convergence of iterative methods, as well as the sensitivity of the solution, can be estimated in terms of the condition number of the system. Hence, we are interested in investigating how the choice of extension factor η_{ext} affects these properties and what would be the ideal choice of this factor, which would result in the preservation of mesh quality during the optimization procedure, while not making the problem too computationally demanding (Figures 1 and 2).

We would like to also remark that despite referring to a computational mesh throughout this section, we actually do not obtain a mesh as a result of the algorithm. After performing the optimization procedure, we obtain the deformation field. Then by using the mapping (8), we compute the deformed mesh in post-processing. This way, we avoid unnecessary generating the mesh at every iteration step and reduce computational cost.

Further to quantify a mesh quality, we choose the mesh quality metric that determines how far we are from an ideal cell shape, that is, an equilateral element in the case of a triangular mesh. In this article, as a measure of the mesh quality, we

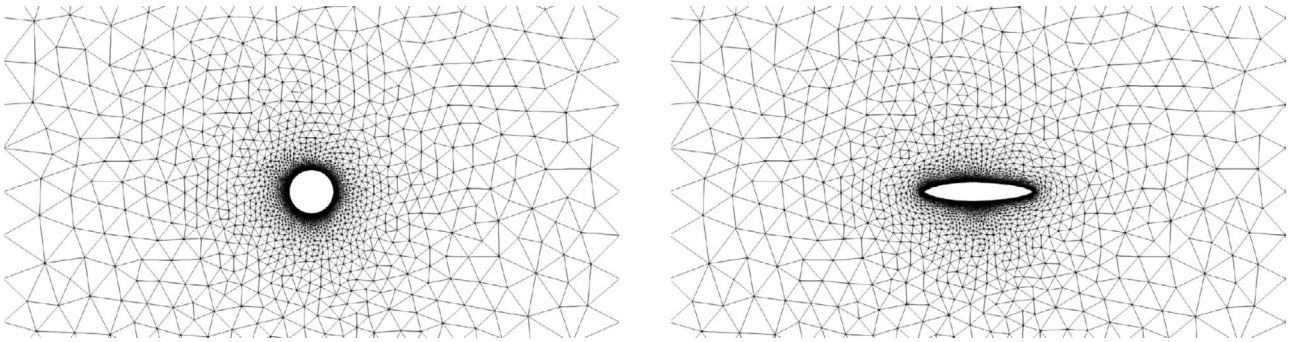

FIGURE 2 Mesh on reference domain and transformed domain, that is, in the optimal solution.

TABLE 1 Iteration counts and mesh quality data for $\eta_{ext} = 0.5$. Condition number of the Hessian of Lagrangian of the problem $\kappa(H) = 119.81$.

Opt. step	RR	RR for tip	Newton	$\frac{j}{j_{init}}$
1	1.81	1.57	6	1
2	1.83	1.56	6	0.9676
3	1.93	1.67	6	0.8814
4	2.58	2.58	6	0.8338
5	5.03	5.03	6	0.8191
6	35.14	34.07	6	0.8113

choose radius ratio (RR), which is computed using the radius of the circumscribing and inscribing circles of the associated element [15, 16]. In the following results, RR refers to the mesh elements of the worst quality, that is, with the largest RR.

Results of the present study are obtained from the open-source toolbox FEniCS Project [17] and dolfin-adjoint [18], which enables automated adjoint models implementation.

In the examples, the computational grid consists of 13 350 triangular elements. We use stable $P2 - P1$ finite elements to discretize the steady nonlinear Navier–Stokes equations (3). The viscosity coefficient is chosen as $\nu = 0.04$, the Tikhonov regularization parameter is set to $\alpha = 1e - 5$, and the determinant condition (Equation 11) parameters $\beta = 10$, and $\eta_{\text{det}} = 0.01$.

In this work, we focus on two particular extension factors: $\eta_{\text{ext}} = 0.5$, $\eta_{\text{ext}} = 1.5$. We do not consider the case $\eta_{\text{ext}} = 0$, since near the front and back tips of the shape (for the chosen set of other parameters, e.g., high low viscosity ν) the cells get compressed and hence the comparison of mesh qualities at the final iteration would be inadequate. Further, we do not consider here significantly larger η_{ext}, since then the problem becomes advection dominated, which leads to an undesirable increase in computational time. For more detailed discussion about corner cases of η_{ext} we refer to Ref. [1].

In Tables 1 and 2, the first column represents the optimization step. The second and third columns contain the RR value for the whole domain and the selected area around the tip of the obstacle, respectively. Further, column four depicts the iteration counts for Newton's method used to solve the extension equation (10). Finally, the last column shows the reduction of the normalized cost functional. We stop the optimization algorithm after the optimal shape was reached and there is no more improvement in the value of the cost functional. Therefore, the amount of optimization steps in Tables 1 and 2 is different, as $\eta_{\text{ext}} = 1.5$ allowed the shape to become more elongated and required more steps (see Figures 3 and 4). Comparing Tables 1 and 2, the improvement in the preservation of mesh quality is observed by choosing a larger extension factor, which leads to a smaller condition number. We also observe a slight rise in the amount of nonlinear iterations for solving the deformation equation and hence computational time. However, this difference is minor. Finally, we remark that the element with the worst RR value in both cases does not belong to the mesh in the area around the tip, which is a clear improvement from the case without nonlinear term, where elements were strongly compressed close to the tip, preventing altogether the tip area from forming. The areas of the mesh where the generation of tips is expected have been chosen to visualize the effects of the deformation field across the computational grid, since it includes the elements that

TABLE 2 Iteration counts and mesh quality data for $\eta_{ext} = 1.5$. Condition number of the Hessian of Lagrangian of the problem $\kappa(H) = 78.65$.

Opt. step	RR	RR for tip	Newton	$\frac{j}{j_{init}}$
1	1.81	1.49	4	1
2	1.83	1.49	5	0.9679
3	1.92	1.57	5	0.8770
4	2.92	2.21	6	0.8174
5	3.24	2.53	7	0.8127
6	3.67	3.04	7	0.8104
7	3.51	2.94	7	0.8102
8	3.52	2.94	7	0.8102
9	3.42	2.81	7	0.8101

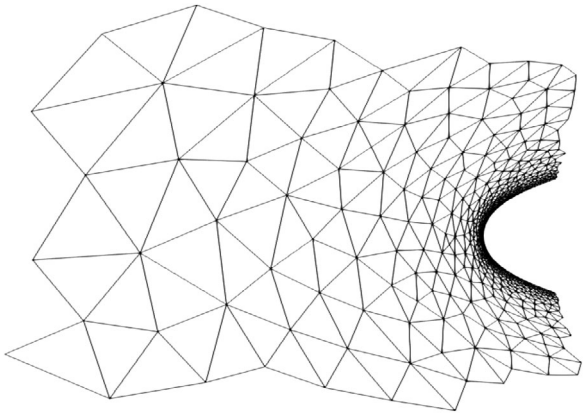

FIGURE 3 Selected area around the front tip of the obstacle at the final optimization step for $\eta_{\text{ext}} = 0.5$ with 1300 elements.

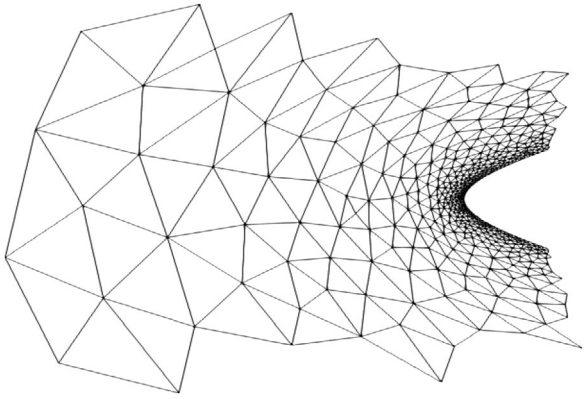

FIGURE 4 Selected area around the front tip of the obstacle at the final optimization step for $\eta_{\text{ext}} = 1.5$ with 1300 elements.

experience the largest deformations. It is seen that the elements close to the surface of the obstacle do not suffer large compression throughout the optimization process.

5 | CONCLUSION

In this work, we illustrated the effects of different choices of extension factors on the numerical properties of shape optimization problems. Our numerical studies indicated that having a nonlinear extension equation, which promotes the movement of nodes towards the tips of the shape, reduces compressed elements in the orthogonal directions, which results in elements of better quality around the boundary of the obstacle. Further, we discussed how the suitable choice of this factor leads to the preservation of mesh quality and hence a lower condition number of the system.

ACKNOWLEDGMENTS

Open access funding enabled and organized by Projekt DEAL.

ORCID

Sofiya Onyshkevych https://orcid.org/0009-0003-8735-4468

REFERENCES

1. Onyshkevych, S., & Siebenborn, M. (2021). Mesh quality preserving shape optimization using nonlinear extension operators. *Journal of Optimization Theory and Applications*, *189*, 291–316.
2. Schmidt, S., Wadbro, E., & Berggren, M. (2016). Large-scale three-dimensional acoustic horn optimization. *SIAM Journal on Scientific Computing*, *38*, B917–B940.

3. Udawalpola, R., & Berggren, M. (2008). Optimization of an acoustic horn with respect to efficiency and directivity. *International Journal for Numerical Methods in Engineering*, *73*(11), 1571–1606.
4. Gangl, P., Laurain, A., Meftahi, H., & Sturm, K. (2015). Shape optimization of an electric motor subject to nonlinear magnetostatics. *SIAM Journal on Scientific Computing*, *37*(6), B1002–B1025.
5. Siebenborn, M., & Welker, K. (2017). Algorithmic aspects of multigrid methods for optimization in shape spaces. *SIAM Journal on Scientific Computing*, *39*(6), B1156–B1177.
6. Pinzon, J., Siebenborn, M., & Vogel, A. (2020). Parallel 3D shape optimization for cellular composites on large distributed-memory clusters. *Journal of Advanced Simulation in Science and Engineering*, *7*(1), 117–135.
7. Hiptmair, R., Scarabosio, L., Schillings, C., & Schwab, C. (2018). Large deformation shape uncertainty quantification in acoustic scattering. *Advances in Computational Mathematics*, *44*, 1475–1518.
8. Delfour, M., & Zolésio, J. P. (2001). *Shapes and geometries: Metrics, analysis, differential calculus, and optimization*. Advances in Design and control (2nd ed., Vol. 22). SIAM.
9. Sokolowski, J., & Zolesio, J. P. (2012). *Introduction to shape optimization: Shape sensitivity analysis*. Springer Science & Business Media.
10. Schulz, V., & Siebenborn, M. (2016). Computational comparison of surface metrics for PDE constrained shape optimization. *Computational Methods in Applied Mathematics*, *16*(3), 485–496.
11. Allaire, G., Dapogny, C., & Jouve, F. (2021). Shape and topology optimization. In A. Bonito & R. H. Nochetto (Eds.), *Geometric partial differential equations, part II*. Handbook of numerical analysis (Vol. 22). Elsevier Science.
12. Haubner, J., Siebenborn, M., & Ulbrich, M. (2021). A continuous perspective on shape optimization via domain transformations. *SIAM Journal on Scientific Computing*, *43*(3), A1997–A2018.
13. Berzins, M. (1999). Mesh quality: A function of geometry, error estimates or both? *Engineering with Computers*, *15*, 236–247.
14. Kim, J., Sastry, S. P., & Shontz, S. M. (2011). A numerical investigation on the interplay amongst geometry, meshes, and linear algebra in the finite element solution of elliptic PDEs. *Engineering with Computers*, *28*(4), 431–450.
15. Caendish, J. C., Field, D. A., & Frey, W. H. (1985). An approach to automatic three-dimensional finite element mesh generation. *International Journal for Numerical Methods in Engineering*, *21*(2), 329–347.
16. Shewchuk, J. (2002). What is a good linear finite element? - Interpolation, conditioning, anisotropy, and quality measures. In Proceedings of the 11th International Meshing Roundtable (Vol. *73*).
17. Logg, A., Mardal, K. A., & Wells, G. (2012). *Automated solution of differential equations by the finite element method: The FEniCS book*. Springer Publishing Company, Incorporated.
18. Farrell, P. E., Ham, D. A., Funke, S. W., & Rognes, M. E. (2013). Automated derivation of the adjoint of high-level transient finite element programs. *SIAM Journal on Scientific Computing*, *35*(4), C369–C393.

How to cite this article: Onyshkevych, S., Siebenborn, M., & Wollner, W. (2023). Preserving mesh quality in shape optimization. *Proceedings in Applied Mathematics and Mechanics*, e202300146. https://doi.org/10.1002/pamm.202300146